Crossover between quantum and classical waves and high-frequency localization landscapes

David Colas ⬤, Cédric Bellis ⬤, Bruno Lombard, and Régis Cottereau ⬤*
Aix Marseille Univ, CNRS, Centrale Marseille, LMA UMR 7031, Marseille, France

Anderson localization is a universal interference phenomenon occurring when a wave evolves through a random medium and it has been observed in a great variety of physical systems, either quantum or classical. The recently developed localization landscape theory offers a computationally affordable way to obtain useful information on localized modes, such as their location or size. Here we examine this theory in the context of classical waves exhibiting high-frequency localization and for which the original localization landscape approach is no longer informative. Using the so-called Webster's transformation, to convert a classical wave equation into a Schrödinger equation with the same localization properties, and combining a set of frequency-shifted operators, we introduce an optimized localization landscape. This optimized localization landscape offers an affordable way to reveal key information on mode localization across the frequency spectrum.

I. INTRODUCTION

Anderson localization AL refers to wave localization due to the presence of a strongly inhomogeneous medium. Originally predicted by P. W. Anderson in 1958 for electronic wave functions [1,2], this phenomenon was since evidenced in a great variety of oscillatory systems, such as electromagnetic [3–5] or matter waves [6–8], in the context of meta-materials [9], photonic lattices [10] or cavity QED [11]. Recently, an attempt at AL measurement involving Bose-Einstein condensates was conducted [12], but the observation have not been reproduced yet. AL has also been studied for classical vibrating systems, mostly for ultrasounds [13–17]. Notable differences exist in the mathematical structure of the operators describing classical and quantum waves, and the general properties of AL, such as the link between the presence of spectral gaps and the emergence of localized modes, are still discussed [18–20]. Despite the abundant literature produced over six decades, many questions on the nature of AL remain open. One important concern is the following: is it possible to determine, from the knowledge of the random medium configuration, where waves are going to localize? And this, without solving the computationally expensive associated eigenvalue problem.

In 2012, M. Filoche and S. Mayboroda developed an original and innovative tool to apprehend wave localization, which they coined as the *localization landscape* [21]. For a given quantum potential $V(x)$, possibly random, one considers the eigenvalue problem for the Schrödinger equation in a domain Ω

$$(-\Delta + V(x))\psi_n(x) = E_n\psi_n(x), \quad \psi_n|_{\partial\Omega} = 0. \quad (1)$$

Instead of Eq. (1), one can solve the elliptic equation

$$(-\Delta + V(x))u_\psi(x) = 1, \quad u_\psi|_{\partial\Omega} = 0, \quad (2)$$

with u_ψ the so-called localization landscape (LL). When analyzing the LL's shape, i.e., its peaks and valleys, one can predict the position, shape and energy of the low-energy localized eigenstates, to a certain extent, and, of course, without solving the eigenvalue problem of Eq. (1). The LL can actually be understood as the inverse of an effective confining potential for the eigenmodes [22], and it has been successfully applied in various contexts [23–30].

This remarkable theory is also extendable to localization associated with other symmetric elliptic differential operators governing wave propagation, such as the Laplacian, the bilaplacian or the operator $-\text{div}(A(x)\nabla)$, notably describing classical waves in inhomogeneous media. However, as we will show, the LL only returns useful information in the case of low frequency localization. When the system exhibits high-frequency localization, i.e., when the first eigenmodes are delocalized, the LL does not bring any insight on the position or shape of the localized modes. Such situation might occur upon the choice of the differential operator or the boundary conditions. Similar observations were reported in Ref. [31] and a first attempt was considered to extend the localization landscape to higher frequencies in a discrete tight-binding Schrödinger model. However, the proposed technique heavily relies on the discreteness of the system and on symmetry properties of the tight-binding model, and hence cannot be applied in the more general case we are interested in. Another interesting attempt to capture high-energy localized states has been recently conducted with the introduction of a modified LL computed from a computationally expensive partial inversion of a Hamiltonian-based matrix [32].

In this paper, we adapt the localization landscape theory (LLT) to classical scalar waves exhibiting high-frequency localization, using as example of a classical wave equation the Helmholtz equation governing acoustics. For a given type of random quantum potential or acoustic structure, we first review and compare the phenomenology associated with the quantum and classical systems, which is essentially an opposite transition between the localization and delocalization
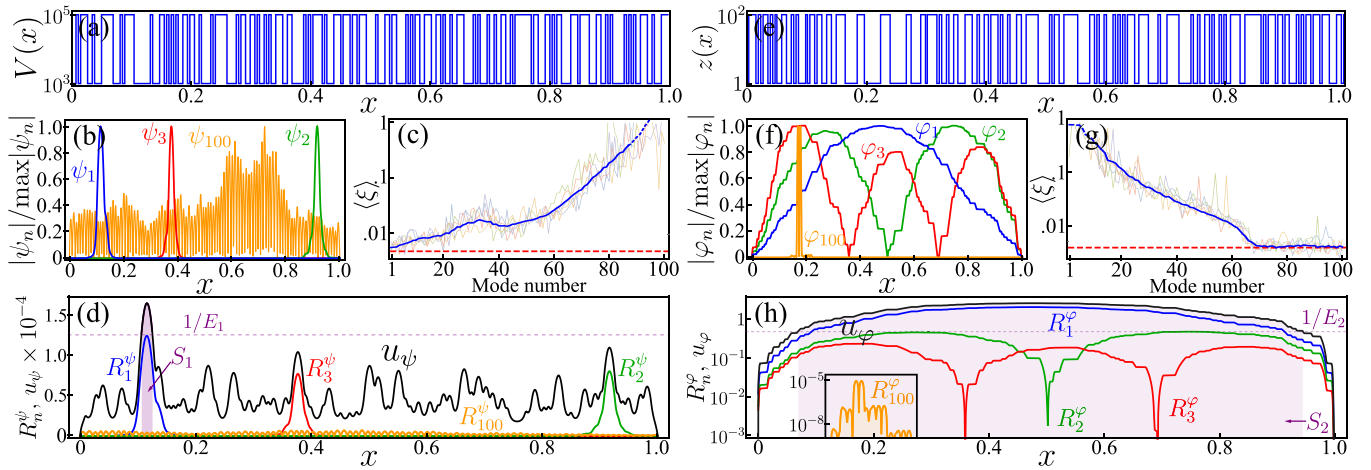
*regis.cottereau@cnrs.fr

FIG. 1. Comparison of mode localization between a quantum [(a)–(d)] and a classical scalar system [(e)–(h)]. [(a) and (e)] Random Bernoulli-type quantum potential $V(x)$ and classical parameter $z(x)$ with $N = 256$ sites. [(b) and (f)] Selection of eigenmodes normalized to their max, for the quantum and classical system, respectively. [(c) and (g)] Mode localization length $\langle \xi \rangle$, averaged on 1000 realizations (blue lines) along with some single realizations. The dash part of the blue curves indicates that the exponential fit is less relevant when modes are delocalized [33]. The dashed-red line set at $1/256$ defines the smallest possible localization site, hence the limit value for $\langle \xi \rangle$. [(d) and (h)] Same selection of modes, now normalized to their energy [R_n^ψ and R_n^φ, see Eq. (3)] and bounded by the corresponding LLs u_ψ and u_φ (black lines). The purple-shaded areas correspond to the supports S_1^ψ and S_2^φ for the modes ψ_1 and φ_2, defined by Eq. (4). An animation of (d) and (h) is provided in Ref. [34].

regimes. Then, we make use of the Webster's transformation [35,36] to symmetrize and convert the Helmholtz equation into a Schrödinger equation with an equivalent random potential that preserves the localized nature of high-energy modes. From that, we build an optimized LL to retrieve information on the original classical modes and their support. This work highlights limitations of the original LLT for systems exhibiting high-frequency localization and enriches it by restoring the LL as a predictive and computationally affordable tool to treat AL.

The paper is organized as follows. Section II illustrates the issue of the lack of effectiveness of the LL for mode localization in classical systems by comparing localized modes in a quantum and classical systems. In Sec. III, we develop an optimized version of the LL, suitable to detect high-frequency localized states. In Sec. IV, we discuss in more details several key aspects of our optimized LL: computational efficiency, applicability to general acoustical systems, and physical meaning of our proposal. Finally, Sec. V concludes the paper.

II. COMPARISON BETWEEN QUANTUM AND CLASSICAL WAVE LOCALIZATION

We start our analysis by examining the phenomenological differences between localization of quantum and classical waves, see also Ref. [37] for more comparisons. We first consider the 1D Schrödinger eigenvalue problem of Eq. (1) with a continuous Bernoulli-type random potential $V(x)$ constructed as follows: a unit-length space is divided into N segments on which V either takes the value $V_{\min}$ or $V_{\max}$, with equiprobability. An example of possible realization with 256 segments is shown in Fig. 1(a). We then calculate the first 100 eigenmodes and show a selection of them in Fig. 1(b). Localized modes are expected to decay exponentially as $|\psi_n(x)| \sim \exp(-x/\xi)$,

with ξ the localization length. In Fig. 1(c), we show the value $\langle \xi \rangle$ fitted for each mode and averaged over a thousand realizations [33]. First modes are indeed localized and delocalization progressively occurs at higher energies. This is typical of a low-energy localization system. We then compute the LL u_ψ from Eq. (2) and present it in Fig. 1(d). One can see the effectiveness of the LLT, with the matching between the LL's main peaks and the first localized modes. The mathematical essence of the LLT is encapsulated in the following inequality [21]:

$$R_n^\psi \stackrel{\text{def}}{=} \frac{|\psi_n(x)|}{\max_\Omega |\psi_n(x)| E_n} \leqslant u_\psi(x). \tag{3}$$

Practically, R_n^ψ represents the mode $|\psi_n(x)|$ normalized by its peak value and its energy. Therefore, the inequality of Eq. (3) states that the LL $u_\psi > 0$ acts as a maximum and bounds the normalized eigenmodes.

In Fig. 1(d), we show how the LL acts as an upper bound for the normalized modes R_n^ψ. Moreover, an eigenmode ψ_n with energy E_n possesses the following approximate support [38]:

$$S_n^\psi \stackrel{\text{def}}{=} \left\{ x \in \Omega : u_\psi(x) \geqslant \frac{1}{E_n} \right\}. \tag{4}$$

In other words, the support S_n^ψ defines where most of a mode's "mass" must sit, as illustrated in Fig. 1(d). As E_n increases with n, eigenmodes are allowed to occupy a larger region of space and thus to delocalize. These mathematical tools constitute the core of the LLT and the way to predict the position and the spatial extent of the localized modes.

We now perform the same analysis with a classical system, taking the example of the 1D scalar wave equation

$$-\frac{1}{\rho(x)} \nabla \cdot (\kappa(x) \nabla \varphi_n(x)) = E_n \varphi_n(x), \tag{5}$$

where $\rho(x)$ and $\kappa(x)$ can be interpreted as a mass density and bulk modulus in the context of acoustics, and the eigenvalues E_n represent frequencies squared (they are usually denoted ω_n^2 but we stick to our notation E_n to simplify the comparison with Schrödinger systems). Note that in this form, the operator in the left-hand side of Eq. (5) is not self-adjoint but could be rewritten as a generalized eigenvalue problem. We further simplify this problem by considering a single random variable, setting $\rho(x) = \kappa(x) = z(x)$. This model is known as the Webster's horn equation [35,36] and as we will see later on, can be easily mapped into a Schrödinger equation. This configuration readily extends to the case where $\kappa(x) = \alpha\rho(x)$, where α is a (positive) constant, by simply rescaling the eigenvalue E_n. This choice will be discussed in Sec. IV. The random parameter $z(x)$ is constructed in the same way as for $V(x)$, and can take the values $z_{\min}$ or $z_{\max}$, see Fig. 1(e). A selection of eigenmodes for Eq. (5) is shown in Fig. 1(f) along with the averaged measurement of their localization length $\langle\xi\rangle$. Unlike for the Schrödinger system, the first modes are fully delocalized and localization progressively occurs at higher energies, see Fig. 1(g), until $\langle\xi\rangle$ reaches the minimal possible value allowed by the system, that is the size of a single site $1/N$. This is typical of a high energy localization system. In Appendix A, we briefly show that for a homogeneous 2D problem, the choice of boundary conditions can also lead to a modification of the localization regime.

The phenomenological difference between the quantum and classical systems can be intuitively understood from the structure of Eqs. (1) and (5). We refer to the argument presented in Ref. [39], which essentially states that for the Schrödinger equation, the potential term is additive to the energy, so that a quantum wave predominantly perceives the effect of the disordered potential at low energies, thus exhibiting low-energy mode localization. On the other hand, the classical wave equation can be rewritten in the form of a Laplacian plus another term, equivalent to a potential, but multiplicative to the energy. At low energy, a classical wave thus essentially perceives a homogeneous medium, and the first eigenmodes resemble the usual global modes of the domain [40], see Fig. 1(f). The random fluctuations become predominant only at higher energies, allowing AL.

We then attempt to compute an equivalent LL for the classical system, for this purpose we solve

$$-\frac{1}{z(x)}\nabla\cdot(z(x)\nabla u_\varphi(x)) = 1, \qquad (6)$$

and show the solution u_φ in Fig. 1(h) along with a selection of normalized modes R_n^φ. Despite the bound $R_n^\varphi \leqslant u_\varphi$ being seemingly valid, u_φ does not here provide any useful information about the mode localization. It is akin to the first eigenmode of the system, and does not possess any peaks or valleys. The higher-energy modes, regardless of their localization, rapidly fall orders of magnitude below u_φ. Equivalently, the support S_n^φ for the first modes already represents a large region of space and quickly converges to the whole domain Ω as the eigenvalue increases ($1/E_n$ decreases). The solution u_φ thus fails to provide information when the first modes of the system are delocalized.

III. OPTIMIZED LOCALIZATION LANDSCAPE FOR HIGH-FREQUENCY LOCALIZATION

The inability of the original LL to detect high energy mode localization brings the need for an updated formulation. To do so, we first use a symmetrized version of the classical wave equation in order to convert it into an equivalent Schrödinger equation. The transformation implies a simple mapping between the two systems as we set $\psi_n(x) = \sqrt{z(x)}\varphi_n(x)$, which leads to

$$-\frac{1}{\sqrt{z(x)}}\nabla\cdot\left(z(x)\nabla\frac{\psi_n(x)}{\sqrt{z(x)}}\right) = E_n\psi_n(x). \qquad (7)$$

Expanding the left-hand side of Eq. (7), one obtains the Laplacian operator and the equivalent potential

$$V_{eq}(x) = \frac{1}{2}\left(\frac{\Delta z}{z} - \frac{|\nabla z|^2}{2z^2}\right), \qquad (8)$$

see Appendix B for details of the transformation.

Such a transformation is notably known as the Webster's transformation [35,36]. It preserves the energy spectrum and only affects the eigenmodes' shape, here modulated by the factor $\sqrt{z}$, see Fig. 2(a) for the first transformed mode. Hence, a localized mode modulated by the delocalized function $\sqrt{z(x)}$ remains localized in the transformed basis, under the reasonable hypothesis that the function $\sqrt{z(x)}$ does not grow exponentially with x. Incidentally, this transformation reveals an interesting fact: one can actually construct a quantum potential $V_{eq}(x)$, although quite nonintuitive, see Fig. 4(e), which leads to high energy mode localization and consequently to an uninformative LL.

We thus adapt the LL by adding an energy shift E_s to the operator in Eq. (7), affecting the eigenvalues but not the eigenstates, and we compute the corresponding LL $\bar{u}_\psi(x; E_s)$:

$$-\frac{1}{\sqrt{z(x)}}\nabla\cdot\left(z(x)\nabla\frac{\bar{u}_\psi(x)}{\sqrt{z(x)}}\right) + E_s\bar{u}_\psi(x) = 1. \qquad (9)$$

Expressing this equation back into the original space through inverse Webster's transform, we obtain the final expression for the shifted LL $\bar{u}_\varphi(x; E_s)$:

$$-\nabla\cdot(z(x)\nabla\bar{u}_\varphi(x; E_s)) + E_s\bar{u}_\varphi(x; E_s)z(x) = \sqrt{z(x)}. \qquad (10)$$

We therefore derive an adapted bound for the original classical modes

$$\bar{R}_n^\varphi(E_s) \stackrel{\text{def}}{=} \frac{|\varphi_n(x)|}{\max_\Omega|\sqrt{z(x)}\varphi_n(x)|(E_n + E_s)} \leqslant \bar{u}_\varphi(x; E_s), \qquad (11)$$

and an adapted expression for their support

$$\bar{S}_n^\varphi(E_s) \stackrel{\text{def}}{=} \left\{x \in \Omega : \bar{u}_\varphi(x; E_s) \geqslant \frac{1}{(E_n + E_s)\sqrt{z(x)}}\right\}. \qquad (12)$$

In Figs. 2(a)–2(c), we show the supports $\bar{S}_n^\varphi(E_s)$ of the first transformed mode $n = 1$, which is delocalized, as well as those of the localized modes $n = 66$ and 70. The supports $\bar{S}_n^\varphi(E_s)$ are computed from Eq. (12) with $E_s = 2 \times 10^4$. As with the original landscape ($E_s = 0$), the shifted landscape does not provide any insight concerning the modes that are delocalized at low energies, see Fig. 2(a). However, contrarily to the original landscape, the introduction of a nonzero shift
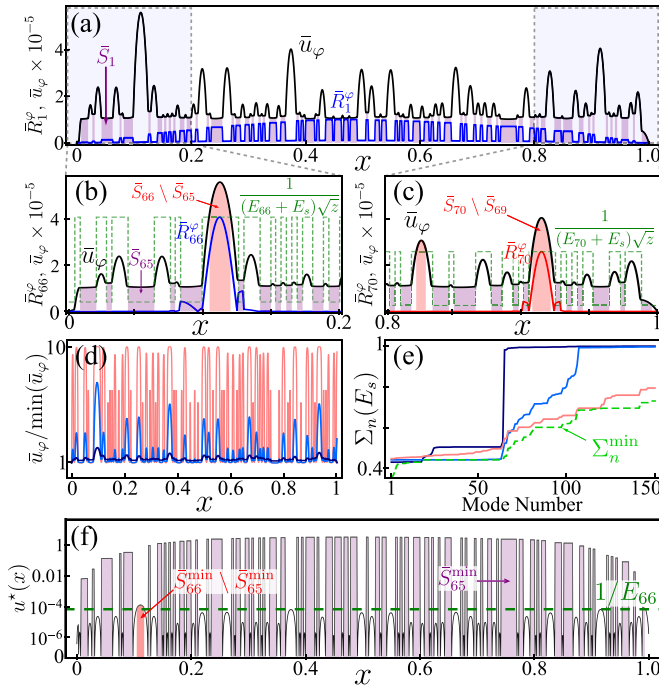
FIG. 2. (a) Shifted LL $\bar{u}_\varphi(x; E_s)$ (black) computed with $E_s = 2 \times 10^4$, and bound for the first eigenmode $\bar{R}_1^\varphi(E_s)$ (blue). Purple-shaded areas correspond to the support $\bar{S}_1^\varphi(E_s)$ defined in Eq. (12). [(b) and (c)] Focus on bounds of the localized modes $\bar{R}_{66}^\varphi(E_s)$ and $\bar{R}_{70}^\varphi(E_s)$. The dashed-green line corresponds to the right-hand side of the inequality in Eq. (13) which locally defines the mode's support. The red-shaded area indicates the extra support obtained from the previous eigenvalue. (d) Evolution of the shifted LL $\bar{u}_\varphi(x; E_s)$ (re-scaled) for different values of energy shift $E_s \in \{10^3, 2 \times 10^4, 10^6\}$ (blue to red). (e) Measure $\Sigma_n^\varphi(E_s)$ of mode support for the same values of shifts E_s as in (c), and measure of the minimum support $\Sigma_n^{\min}$ (dashed-green). (f) Function $u^\star(x)$ defining the minimal mode support (black). The purple-shaded area is the support for the 65th eigenvalue while the red-dashed area indicates the extra support obtained for the 66th one. An animation of (a) and (f) for a set of modes is provided Ref. [34].

$E_s > 0$ now reveals information on the modes that are localized at high energies, see Figs. 2(b) and 2(c). We emphasize that the shifted LL $\bar{u}_\varphi$ can be computed for an arbitrary energy shift E_s. Yet, the choice of E_s has a strong influence on the LL's final shape, and on its capacity to reveal information on localized modes in a given range of energy. For a small shift ($E_s \to 0$), the LL remains uninformative as it is akin to a global structure mode [40], as in Fig. 1(h). In the limit of large shifts ($E_s \to +\infty$) the LL converges to the medium's structure ($\bar{u}_\varphi \to 1/\sqrt{z}$). In the first limit the LL does not possess any peaks or valleys, and in the second limit all peaks or valleys have the same values, which is uninformative in both cases. Only intermediary values of E_s lead to a useful landscape with distinct local maxima, as shown in Fig. 2(d) where $\bar{u}_\varphi(x; E_s)$ is plotted for different values of E_s.

To finally get rid of the arbitrary choice of E_s, we propose a method to compute a minimal support $\bar{S}_n^{\varphi,\min}$ for each mode. We have seen that a mode φ_n must be mostly located in the support $\bar{S}_n^\varphi(E_s)$ defined by Eq. (12), and this, for all values of E_s. By contraposition, we can state that if, at a given position

x, there exists a shift E_s for which Eq. (12) is not satisfied, then x must be excluded from $\bar{S}_n^{\varphi,\min}$. So for every point of the domain Ω and at a given energy level E_n of interest, one can simply check among a previously calculated set of landscape functions $\bar{u}_\varphi(x; E_s)$, if there is a value E_s for which Eq. (12) is not satisfied. In such case this position is excluded from the support of the mode φ_n. This procedure amounts in computing the intersection of all mode supports associated with the considered shifts, and it defines the minimal support for the modes

$$\bar{S}_n^{\varphi,\min} = \left\{ x \in \Omega : u_\varphi^\star(x) \geqslant \frac{1}{E_n} \right\}, \quad (13)$$

with the optimized LL function defined as

$$u_\varphi^\star(x) = \left(\max_{E_s} \left\{ \frac{1}{\bar{u}_\varphi(x; E_s)\sqrt{z(x)}} - E_s \right\} \right)^{-1}. \quad (14)$$

We emphasize that the optimization in this definition is performed locally for each x, so that the value of the optimal $u_\varphi^\star(x)$ in different positions might correspond to different E_s. In order to understand which values of the shift give information on localized states, we show in Fig. 2(e) the measure $\Sigma_n(E_s) = \int_\Omega \bar{S}_n^\varphi(E_s) dx$ of the mode support for different values of shift, along with the measure of the minimal support $\Sigma_n^{\min} = \int_\Omega \bar{S}_n^{\varphi,\min} dx$. This highlights the drawback in using a single shift value E_s: the landscape $\bar{u}_\varphi(x; E_s)$ and support $\bar{S}_n^\varphi(E_s)$ only provide useful information in a certain range of energies (or mode number). Above this value, $\Sigma_n(E_s)$ converges to the whole domain Ω, hence being not informative anymore. This confirms the interest of the proposed approach where an optimal shift is locally found numerically to recover the most information.

The function $u_\varphi^\star$ defining the minimal support and the example of the minimal support for the 66th mode are presented in Fig. 2(f). It clearly shows how low-energy modes possess an extended support (purple-shaded areas) and how extra supports (red-shaded area) for the localized mode appear at higher energies. Equations (13) and (14) arise as a powerful tool to predict the position of high-energy localized states as well as the energy at which these localized modes appear.

IV. DISCUSSION

In the following discussion, several remarks on the proposed methodology are in order.

(a) Use of Webster's transform and universality of the considered acoustical system. In our proposal, we have limited our attention to acoustical systems for which $\kappa(x) = \alpha\rho(x)$ where α is a constant. This case includes the important realistic situation of a composite structure whose constituents belong to a class of materials with identical ratios κ/ρ. Outside of such classes, Webster's technique is not sufficient to transform the acoustic equation into a Schrödinger equation, and more general transformation must be considered, these more complex transformations notably involve mappings of coordinates [41,42] and will be described in a forthcoming paper. Note that we choose to transform the original classical wave equation into a Schrödinger equation in order to readily apply the theoretical arguments of [38] to characterize the eigenmodes by a relationship such as Eq. (12).

(b) Physical meaning of the shift in Eq. (10). In our proposal, the original operator is shifted by a positive energy E_s. The reason for this shift to be positive is that using a negative shift would result in a shifted operator that would not verify a maximum principle so that a bound of the form of Eq. (12) could not be retrieved. However, it is interesting to note that the most classical numerical algorithms to derive eigenvalues, such as the Rayleigh-Ritz algorithm, are iterative procedures where the operator is shifted through negative energies to induce resonance around a given eigenvalue, where the response of the system is mostly governed by the associated eigenmode. Clearly, the phenomenon that is induced with our shifted operator is not resonance. Besides, the optimization of Eq. (14) involves not only the solution $\bar{u}_\varphi(x; E_s)$ of the shifted operator but again a shift (negative this time). The overall phenomenon at play here is therefore quite different, and remains to be investigated further.

(c) Computational cost. The original LLT has the enormous advantage of revealing information on (low-energy) mode localization by solving one elliptic problem, with a computational complexity of $\mathcal{O}(M \log M)$ [31,43], instead of solving an eigenvalue problem, with a computational complexity of $\mathcal{O}(M^2 \log M)$. In these comparisons, M is the size of the system (number of sites in a discrete setting, or number of discretization nodes in a numerical approximation of a continuous system), and sparsity of the resulting matrix has been assumed. Although our method is less efficient than the original [21], in the sense that a user-chosen number (say, m) of elliptic problems need to be solved instead of just one, it is still much more efficient than solving an eigenvalue problem, as for large M, $\mathcal{O}(mM \log M) \ll \mathcal{O}(M^2 \log M)$, as long as m is not dependent on M, as seem to indicate our numerical experiments.

(d) Are low-energy modes of the Schrödinger equation always localized ? Although this is not the main objective of this paper, it is interesting to note that, through the Webster's transform, we have explicitly constructed a potential for a Schrödinger equation for which the low-energy modes are delocalized, and localization occurs at higher energies. We believe that this approach might provide a strategy for constructing potentials that yield localization at some specific energy levels.

V. CONCLUSION

In conclusion, we have shown that, although being mathematically valid for classical waves, the LLT is not appropriate to describe high-energy AL. The LLT is therefore not well suited to describe localization in classical systems, and even in some quantum systems, such as the one derived in this paper. The inversion of the usual localization/delocalization phenomenology greatly complicates the analysis of localized modes and the prediction of their position and shape. We have introduced an optimized LL, combining a nonuniform excitation of the system and an optimization process over a set of positively shifted operators, which allows to recover information on localized modes. The minimal support for each mode can then be constructed by combining landscape functions computed from these different energy shifts. This is of course computationally more expensive than solving a
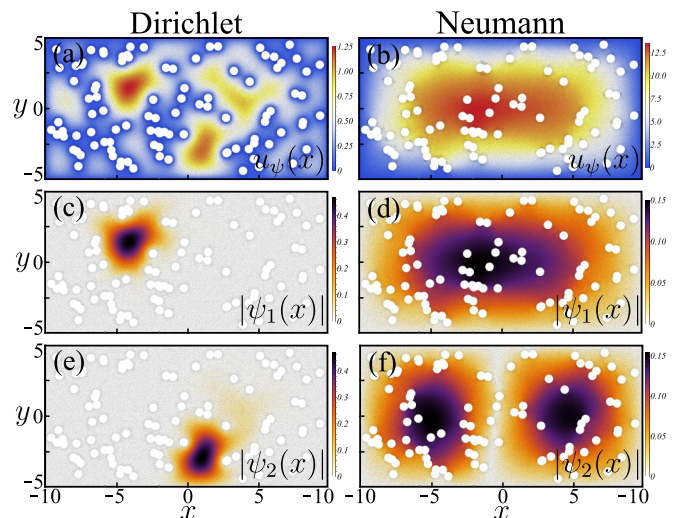

FIG. 3. Effect of boundary conditions on mode localization for a 2D homogeneous surface randomly pierced with holes. Left column corresponds to homogeneous Dirichlet BCs on all boundaries. Right column corresponds to homogeneous Dirichlet BCs on the external domain boundaries and homogeneous Neumann BCs on the boundaries of the holes. [(a) and (b)] Localization landscape u_ψ. First [(c) and (d)] and second [(e) and (f)] eigenmodes.

single elliptic problem but remains, in practice, an advantageous alternative to solving the original eigenvalue problem [43]. Although the optimized LLT was derived here in the case of an acoustic model for which the material parameters verify $\kappa(x) = \alpha \rho(x)$ to simplify the mathematical derivations, the more general case will be described in a forthcoming paper.

APPENDIX A: EFFECT OF BOUNDARY CONDITIONS ON 2D WAVE LOCALIZATION

We provide a concrete and illustrative example of the effect of the boundary conditions (BCs) on the mode localization for a homogeneous 2D surface randomly pierced with holes. We always assume homogeneous Dirichlet BCs on the edge of the 2D domain and we either consider homogeneous Dirichlet or homogeneous Neumann BCs on the edges of the holes. Using a finite-element method, we compute the first modes for the eigenvalue problem $-\Delta \psi_n = E_n \psi_n$ and the associated LLs $-\Delta u_\psi = 1$, with the corresponding BCs. The LLs along with the two first modes for each case are shown in Fig. 3. The case with homogeneous Dirichlet BCs everywhere is analog to the one presented in Ref. [21] and exhibits low-frequency mode localization, with the main peaks of the LL indicating the position and shape of the first localized eigenmodes, see panels (a), (c), and (e). However, with homogeneous Neumann BCs on the edges of the holes, the first modes are essentially unaffected by the presence of holes and thus they

are delocalized. The LL is akin to the first global structure mode, so uninformative, see panels (b), (d), and (f).

APPENDIX B: WEBSTER'S TRANSFORMATION

The Webster's transformation maps a one-parameter classical wave equation into a time-independent Schrödinger equation. Starting from

$$-\frac{1}{z(x)}\nabla \cdot (z(x)\nabla\varphi_n(x)) = E_n\varphi_n(x) \qquad \text{(B1)}$$

and introducing $\psi_n(x) = \sqrt{z(x)}\varphi_n(x)$ yields

$$-\frac{\Delta\psi}{\sqrt{z}} + \frac{1}{2z\sqrt{z}}\left(\Delta z - \frac{|\nabla z|^2}{2z}\right)\psi = E_n\left(\frac{\psi_n}{\sqrt{z}}\right). \qquad \text{(B2)}$$

Simplifying by $\sqrt{z}$, and introducing the equivalent potential

$$V_{\text{eq}}(x) = \frac{1}{2}\left(\frac{\Delta z}{z} - \frac{|\nabla z|^2}{2z^2}\right) \qquad \text{(B3)}$$

eventually leads to a Schrödinger equation for $\psi(x)$:

$$-\Delta\psi_n(x) + V_{\text{eq}}(x)\psi_n(x) = E_n\psi_n(x). \qquad \text{(B4)}$$

The eigenvalue E_n is both the eigenfrequency (squared) corresponding to the eigenmode $\varphi_n(x)$ of the original acoustic equation and the eigenenergy corresponding to the eigenmode $\psi_n(x)$ of the resulting Schrödinger equation.

Since the definition in Eq. (B3) involves differentiation of the material parameter z, care must be taken with discontinuous parameters (as in the examples of this paper). In that case, the procedure described in Appendix C can be used.

APPENDIX C: ACOUSTIC STRUCTURE AND ASSOCIATED POTENTIAL

The Bernoulli-type random parameter $z(x)$ that we previously considered essentially consists in a succession of rectangle functions with different widths, see Fig. 1(e). Practically, to numerically construct our classical 1D random structure $z(x)$, we choose a smoothed approximation of rectangular functions based on *error* functions. At a site k, we
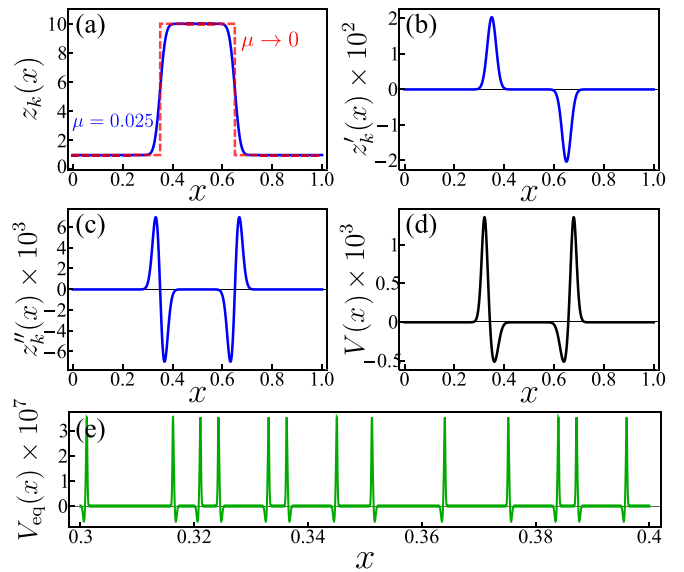

FIG. 4. (a) Example of a basis function $z_k(x)$ for a single site, centered at $x_k = 0.5$, with $z_{\text{max}} = 10$, $z_{\text{min}} = 1$ and a width $\sigma = 0.3$. With $\mu = 0.025$ edges are smoothed (blue line), and the original rectangle function is recovered with $\mu \to 0$ (dashed-red line). (b) First derivative of $z_k(x)$, that is a sum of two Gaussian functions of opposite sign. (c) Second derivative of $z_k(x)$. (d) Quantum potential obtained from $z(x)$, see Eq. (8), possessing both a positive and negative part. (e) Section of the effective potential computed with the parameter $z(x)$ from Fig. 1(e).

thus have

$$z_k(x) = \frac{z_{\text{max}} - z_{\text{min}}}{4}\left[\text{erf}\left(\frac{x + \sigma_k/2 - x_k}{\mu} + 1\right) \right.$$
$$\left. \times \text{erf}\left(\frac{-x + \sigma_k/2 + x_k}{\mu} + 1\right)\right], \qquad \text{(C1)}$$

shaping a smooth rectangle function of height z_{max}, centered at a position x_k and with width σ_k. The parameter μ controls the smoothness of the rectangle's walls, assuming $0 < \mu \ll \sigma$. In the limit of $\mu \to 0$, $z_k(x)$ defines a straight rectangle function. This choice is particularly convenient for the derivation and the numerical computation of the Webster's equivalent potential $V_{\text{eq}}(x)$, see Eq. (8), since it essentially involves first and second derivatives of $z(x)$. In our approximation, they end up being Gaussian and first derivative of Gaussian functions, instead of Dirac delta functions and their derivatives if sharp rectangle functions are chosen. The rectangle ($\mu \to 0$) and smoothed rectangle functions ($\mu > 0$) are plotted in Fig. 4(a), along with the first (b) and second derivative (c), for the smoothed case. The potential function from Eq. (8) is shown in Fig. 4(d). A section of the equivalent potential computed from the initial parameter $z(x)$ of Fig. 1(e) is also shown in Fig. 4(e). Performing the Webster's transform leads here to an equivalent potential which resembles a "Gaussian" comb.

[1] P. W. Anderson, Absence of diffusion in certain random lattices, Phys. Rev. **109**, 1492 (1958).

[2] P. Markoš, Numerical analysis of the Anderson localization, Acta Physica Slovaca **56**, 561 (2006).

[3] D. Laurent, O. Legrand, P. Sebbah, C. Vanneste, and F. Mortessagne, Localized Modes in a Finite-Size Open Disordered Microwave Cavity, Phys. Rev. Lett. **99**, 253902 (2007).

[4] T. Schwartz, G. Bartal, S. Fishman, and M. Segev, Transport

and Anderson localization in disordered two-dimensional photonic lattices, Nature (London) **446**, 52 (2007).

[5] F. Riboli, P. Barthelemy, S. Vignolini, F. Intonti, A. D. Rossi, S. Combrie, and D. S. Wiersma, Anderson localization of near-visible light in two dimensions, Opt. Lett. **36**, 127 (2010).

[6] M. Piraud, A. Aspect, and L. Sanchez-Palencia, Anderson localization of matter waves in tailored disordered potentials, Phys. Rev. A **85**, 063611 (2012).

[7] J. Billy, V. Josse, Z. Zuo, A. Bernard, B. Hambrecht, P. Lugan, D. Clement, L. Sanchez-Palencia, P. Bouyer, and A. Aspect, Direct observation of Anderson localization of matter waves in a controlled disorder, Nature (London) **453**, 891 (2008).

[8] B. Shapiro, Cold atoms in the presence of disorder, J. Phys. A.: Math. Theor. **45**, 143001 (2012).

[9] A. A. Asatryan, S. A. Gredeskul, L. C. Botten, M. A. Byrne, V. D. Freilikher, I. V. Shadrivov, R. C. McPhedran, and Y. S. Kivshar, Anderson localization of classical waves in weakly scattering metamaterials, Phys. Rev. B **81**, 075124 (2010).

[10] Y. Lahini, A. Avidan, F. Pozzi, M. Sorel, R. Morandotti, D. N. Christodoulides, and Y. Silberberg, Anderson Localization and Nonlinearity in One-Dimensional Disordered Photonic Lattices, Phys. Rev. Lett. **100**, 013906 (2008).

[11] L. Sapienza, H. Thyrrestrup, S. Stobbe, P. D. Garcia, S. Smolka, and P. Lodahl, Cavity quantum electrodynamics with Anderson-localized modes, Science **327**, 1352 (2010).

[12] D. H. White, T. A. Haase, D. J. Brown, M. D. Hoogerland, M. S. Najafabadi, J. L. Helm, C. Gies, D. Schumayer, and D. A. W. Hutchinson, Observation of two-dimensional Anderson localisation of ultracold atoms, Nat. Commun. **11**, 4942 (2020).

[13] C. A. Condat and T. R. Kirkpatrick, Observability of Acoustical and Optical Localization, Phys. Rev. Lett. **58**, 226 (1987).

[14] R. L. Weaver, Anderson localization of ultrasound, Wave Motion **12**, 129 (1990).

[15] O. I. Lobkis and R. L. Weaver, Anderson localization of ultrasound in plates: Further experimental results, J. Acoust. Soc. Am. **124**, 3528 (2008).

[16] H. Hu, A. Strybulevych, J. H. Page, S. E. Skipetrov, and B. A. van Tiggelen, Localization of ultrasound in a three-dimensional elastic network, Nat. Phys. **4**, 945 (2008).

[17] J. Dhillon, A. Bozhko, E. Walker, A. Neogi, and A. Krokhin, Localization of ultrasound in 2D phononic crystal with randomly oriented asymmetric scatterers, J. Appl. Phys. **129**, 134701 (2021).

[18] T. R. Kirkpatrick, Localization of acoustic waves, Phys. Rev. B **31**, 5746 (1985).

[19] A. Figotin and A. Klein, Localization of classical waves i: Acoustic waves, Commun. Math. Phys. **180**, 439 (1996).

[20] R. Altmann, P. Henning, and D. Peterseim, Quantitative Anderson localization of Schrödinger eigenstates under disorder potentials, Math. Mod. Meth. Appl. S. **30**, 917 (2020).

[21] M. Filoche and S. Mayboroda, Universal mechanism for Anderson and weak localization, Proc. Nat. Acad. Sci. USA **109**, 14761 (2012).

[22] D. N. Arnold, G. David, D. Jerison, S. Mayboroda, and M. Filoche, Effective Confining Potential of Quantum States in Disordered Media, Phys. Rev. Lett. **116**, 056602 (2016).

[23] M. Filoche, M. Piccardo, Y.-R. Wu, C.-K. Li, C. Weisbuch, and S. Mayboroda, Localization landscape theory of disorder in semiconductors. I. theory and modeling, Phys. Rev. B **95**, 144204 (2017).

[24] M. Piccardo, C.-K. Li, Y.-R. Wu, J. S. Speck, B. Bonef, R. M. Farrell, M. Filoche, L. Martinelli, J. Peretti, and C. Weisbuch, Localization landscape theory of disorder in semiconductors. II. urbach tails of disordered quantum well layers, Phys. Rev. B **95**, 144205 (2017).

[25] C.-K. Li, M. Piccardo, L.-S. Lu, S. Mayboroda, L. Martinelli, J. Peretti, J. S. Speck, C. Weisbuch, M. Filoche, and Y.-R. Wu, Localization landscape theory of disorder in semiconductors. III. application to carrier transport and recombination in light emitting diodes, Phys. Rev. B **95**, 144206 (2017).

[26] Y. Chalopin, F. Piazza, S. Mayboroda, C. Weisbuch, and M. Filoche, Universality of fold-encoded localized vibrations in enzymes, Sci. Rep. **9**, 12835 (2019).

[27] S. Balasubramanian, Y. Liao, and V. Galitski, Many-body localization landscape, Phys. Rev. B **101**, 014201 (2020).

[28] G. Lemut, M. J. Pacholski, O. Ovdat, A. Grabsch, J. Tworzydło, and C. W. J. Beenakker, Localization landscape for Dirac fermions, Phys. Rev. B **101**, 081405(R) (2020).

[29] C. Garcia, N. Dauchez, Y. B. de l'Epine, and G. Lefebvre, Localized modes prediction in a membrane with non-uniform tension from the quasi-static measurement of its localization landscape, J. Sound Vibrations **511**, 116272 (2021).

[30] S. S. Shamailov, D. J. Brown, T. A. Haase, and M. D. Hoogerland, Computing the eigenstate localisation length at very low energies from localisation landscape theory, SciPost Phys. Core **4**, 017 (2021).

[31] M. L. Lyra, S. Mayboroda, and M. Filoche, Dual landscapes in Anderson localization on discrete lattices, Europhys. Lett. **109**, 47001 (2015).

[32] L. Herviou and J. H. Bardarson, $\mathcal{L}^2$ localization landscape for highly excited states, Phys. Rev. B **101**, 220201(R) (2020).

[33] Fitting the modes with an exponential becomes irrelevant when they delocalize, i.e., when $\xi \to 1$.

[34] See Supplemental Material at http://link.aps.org/supplemental/10.1103/PhysRevB.106.184210 for videos. Supplementary video S1 corresponds to an animated version of Figs. 1(b), 1(d), 1(f), and 1(h) for the first 100 eigenmodes of the quantum (top) and classical (bottom) systems. Normalized modes $R_{\psi,n}$ and $R_{\varphi,n}$ with their respected localization landscapes and supports are shown on the left. Eigenmodes simply normalized to 1 are shown on the right. Supplementary video S2 corresponds to an animated version of Figs. 2(a)–2(c), and 2(f), also for the first 100 eigenmodes. The first two rows show the adapted landscape $\bar{u}_{\varphi}(x; E_s)$ and the mode support defined by the local condition defined in Eq. (13), with a focus on specific areas. The bottom row shows the function $u^{\star}(x)$ defining the minimum support and its evolution as a function of $1/E_n$ decreases.

[35] A. G. Webster, Acoustical impedance, and the theory of horns and of the phonograp, Proc. Nat. Acad. Sci. USA **5**, 275 (1919).

[36] P. A. Martin, On Webster's horn equation and some generalizations, J. Acoust. Soc. Am. **116**, 1381 (2004).

[37] B. A. van Tiggelen and E. Kogan, Analogies between light and electrons: density of states and Friedel's identity, Phys. Rev. A **49**, 708 (1994).

[38] D. N. Arnold, G. David, M. Filoche, D. Jerison, and S. Mayboroda, Localization of eigenfunctions via an effective potential, Commun. Part. Diff. Eqs. **44**, 1186 (2019).

[39] M. van der Baan, Acoustic wave propagation in one dimensional random media: the wave localization approach, Geophy. J. Int. **145**, 631 (2001).

[40] J. P. Fouque, J. Garnier, G. Papanicolaou, and K. Solna, *Wave Propagation and Time Reversal in Randomly Layered Media* (Springer, New York, USA, 2007).

[41] A. R. Plastino, A. Rigo, M. Casas, F. Garcias, and A. Plastino, Supersymmetric approach to quantum systems with position-dependent effective mass, Phys. Rev. A **60**, 4318 (1999).

[42] J. J. Pena, J. M. E. Zamora-Gallardo, and J. Garcia-Ravelo, Isospectral orthogonal polynomials from the darboux transforms, Int. J. Quantum Chem. **100**, 957 (2004).

[43] G. H. Golub and C. F. van Loan, *Matrix Computations*, 4th ed., Johns Hopkins Studies in the Mathematical Sciences (JHU Press, Baltimore, USA, 2013).